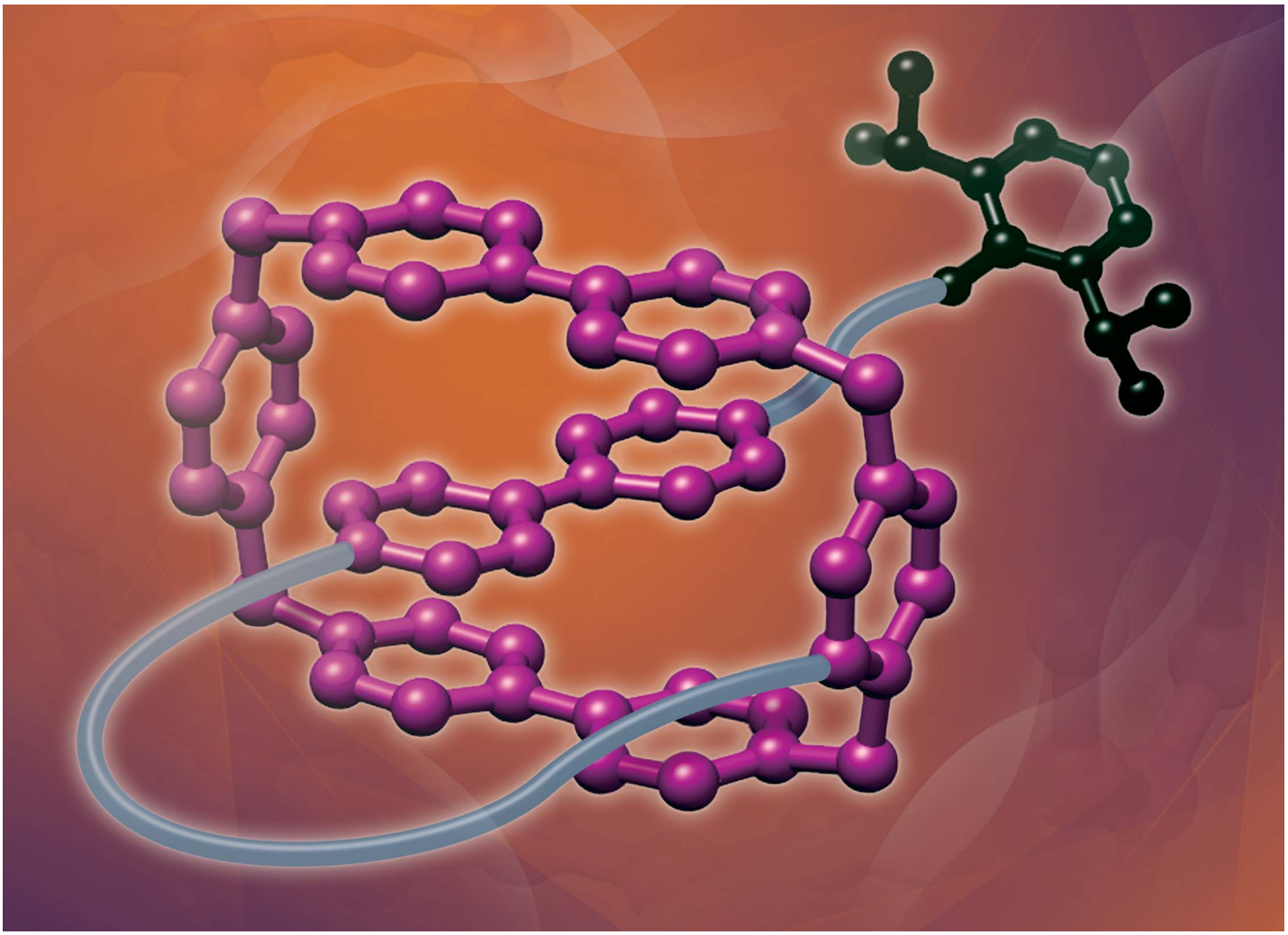

Showcasing research from Sir Fraser Stoddart's laboratory, Department of Chemistry, Northwestern University, Illinois, United States.

Radically promoted formation of a molecular lasso

A viologen-based molecular actuator has been synthesised, and solution studies revealed its stererochemically unambiguous formation of a lasso-like self-entangled conformation by employing either chemical or electrochemical stimuli. In comparison, simply by changing the linker group in this actuator to a bulkier one, the lasso formation is not allowed in the case of the reference compound because of the steric effect. This research shows how tiny structural differences can induce significantly different self-complexing properties and sheds light on designing functional artificial actuators.

As featured in:

See J. Fraser Stoddart *et al.*, *Chem. Sci.*, 2017, **8**, 2562.

ROYAL SOCIETY OF CHEMISTRY

rsc.li/chemical-science

Registered charity number: 207890

Chemical Science

EDGE ARTICLE

View Article Online
View Journal | View Issue

CrossMark click for updates

Cite this: *Chem. Sci.*, 2017, **8**, 2562

Radically promoted formation of a molecular lasso†

Yuping Wang,[a] Junling Sun,[a] Zhichang Liu,[a] Majed S. Nassar,[b] Youssry Y. Botros[bc] and J. Fraser Stoddart*[a]

Received 14th November 2016
Accepted 15th January 2017

DOI: 10.1039/c6sc05035b

www.rsc.org/chemicalscience

Two potential viologen-based molecular lasso precursors—both composed of a 4,4′-bipyridinium ($BIPY^{2+}$) unit as part of a rope appended to a cyclobis(paraquat-*p*-phenylene) ($CBPQT^{4+}$) loop—that have been designed to mimic the threading/unthreading motion of lasso peptides, have been synthesised and characterised. Solution and solid-state experiments reveal that, when the $BIPY^{2+}$ unit in the rope and the $CBPQT^{4+}$ loop are connected by a bulky linker, no lasso-like conformational transformation is observed between the different redox states on account of steric effects. In sharp contrast, when the linker size is small, the molecule can be switched between (i) a free rope-like conformation in its fully oxidised state and (ii) a self-entangled lasso-like conformation under reducing conditions employing either chemical or electrochemical stimuli: the $BIPY^{\bullet+}$ unit in the rope resides inside the cavity of the $CBPQT^{2(\bullet+)}$ loop, forming a pseudo[1]rotaxane. The switching process is reversible and stereochemically unambiguous. This research shows how tiny structural differences can induce significantly different self-complexing properties and sheds light on designing functional artificial actuators.

Introduction

As chemists, we often claim that we draw inspiration from Mother Nature. Lasso peptides,[1,2] which contain 16–21 amino acid residues,[3] constitute members of the ribosomally assembled and post-translationally modified peptides (RiPPs) superfamily.[4] The understanding of their biofunctions[5,6] has attracted the attention of chemists, principally on account of their remarkable stabilities, resulting from their self-entangled conformations. Specifically, composed of macrocycles and axles that thread the macrocycles, lasso peptides exhibit their biological activities by adopting compact—in comparison with their unthreaded analogues—lasso-like conformations. Designing and synthesising abiotic counterparts, not only provides us with wholly synthetic compounds that can mimic the threading-unthreading behaviour[7] of lasso peptides, but it also enriches the family of artificial molecular actuators displaying controllable intramolecular motions. So far, among all the attempts that have been made, (pseudo)[1]rotaxanes,[8–13] which bear (Fig. 1) macrocycles (loops) encircling or otherwise[14] tails that are connected covalently to the loops, have been shown[3] to be promising synthetic targets. Usually, the formation of the mechanically interlocked compounds in the form of (pseudo)[1]rotaxanes are driven by weak interactions such as (i) hydrogen bonds between crown ether[15] and ammonium or triazolium ions,[13,16–18] (ii) hydrophobic forces in water between the cavities of cyclodextrins and aromatic guest substrates,[11,19–21] (iii) metal–ligand coordinative interactions[22] and (iv) donor–acceptor interactions[10,23] between cyclobis(paraquat-*p*-phenylene) ($CBPQT^{4+}$) host and electron-rich tetrathiafulvalene (TTF) and 1,5-dioxynaphthalene (DNP) units. Amongst all the reported examples,[13,22] however, pseudo[1]rotaxanes that are able to switch reversibly between self-entangled and disentangled states remain a rare phenomenon. Moreover, the actuation processes are usually triggered exclusively by chemical stimuli, which inevitably introduces additional species onto the scene and so complicates the situation. In order to avoid all these disadvantages, we have designed a new class of pseudo[1]rotaxane actuated by a different type of noncovalent bonding interaction. Not so long ago, we discovered[24,25] that under reducing conditions, the radical cationic state of the bipyridinium unit, namely $BIPY^{\bullet+}$, interacts strongly with the bisradical dicationic state $CBPQT^{2(\bullet+)}$. Since this radical-mediated recognition has been demonstrated[26,27] to be reversible in solution, upon varying the external applied electro-potential, we decided to take advantage of this recognition to construct pseudo[1]rotaxane-based lassos. It is noteworthy that radical-pairing recognition has also been shown[28] to drive the self-sorting behavior of numerous other organic radicals, *e.g.*, thiazyl radicals.

[a]*Department of Chemistry, Northwestern University, 2145 Sheridan Road, Evanston, Illinois 60208, USA. E-mail: stoddart@northwestern.edu; Tel: +1-847-491-3793*
[b]*Joint Center of Excellence in Integrated Nano-Systems (JCIN), King Abdul-Aziz City for Science and Technology (KACST), P. O. Box 6086, Riyadh 11442, Saudi Arabia*
[c]*PanaceaNano, Inc., 2265 East Foothill Boulevard, Pasadena, California 91107, USA*

† Electronic supplementary information (ESI) available. CCDC 1517068. For ESI and crystallographic data in CIF or other electronic format see DOI: 10.1039/c6sc05035b

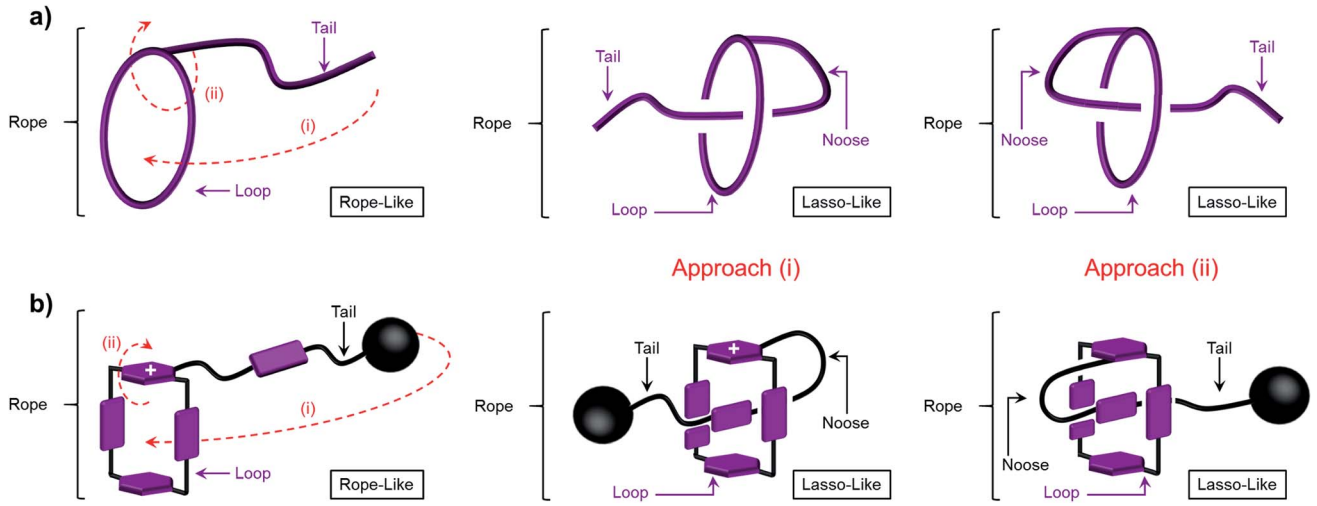

Fig. 1 Illustrations of the transformation of a lasso precursor between its rope-like and lasso-like conformations employing (a) a rope and (b) a graphical representation of $\mathbf{1}^{3(\bullet+)}$ and $\mathbf{2}^{3(\bullet+)}$. The terms we chose for the description in this paper are shown and the two pathways, (i) threading and (ii) self-entanglement approach, are denoted by the red dot lines. It should be noted that in (b), the plane labelled with "+" sign faces up after process (i) and faces down after process (ii).

Results and discussion

When designing the structures of the pseudo[1]rotaxanes, two general mechanisms of actuation come to mind. They involve (Fig. 1) (i) a threading[29] approach where the end of the tail is small enough to go through the cavity of the loop, forming the pseudo[1]rotaxane and (ii) a self-entanglement approach, in which the tail is pulled into the cavity of the loop forming a pseudo[1]rotaxane, as a result of one portion of the loop—*i.e.*, the portion connected to the tail—rotating like a revolving door (Fig. 1b) with respect to the mean plane of the ring.[3,13,22] In both approaches (i) and (ii), the rope-like conformations are converted into the lasso-like conformations, while forming (Fig. 1) nooses at the same time. Although the second one—namely the revolving-door mechanism—is less obvious, it can be considered as a viable pathway since it is not necessary for the entire tail portion to pass through the cavity of the loop during the revolving process. As a result, the tail can be substituted by a bulky group with some desired function, such that, not only will it stand a good chance of introducing new properties into the pseudo[1]rotaxane, but it will also exclude the possibility of intermolecular complexation, *e.g.*, daisy chain-style oligomer formation.[12,30–32] On the basis of these considerations, we report (Scheme 1) herein how $\mathbf{1}^{6+}$ and $\mathbf{2}^{6+}$ were prepared by Cu(I)-catalysed alkyne-azide cycloadditions (CuAAC) between (i) a $BIPY^{2+}$-based half-dumbbell component $\mathbf{5}^{2+}$—in which one end is functionalised with a 2,6-diisopropylphenyl group to act as a stopper—and (ii) a couple of alkyne-functionalised $CBPQT^{4+}$ derivatives $\mathbf{3}^{4+}$ and $\mathbf{4}^{4+}$, respectively. The resulting molecular-lasso precursors $\mathbf{1}^{6+}$ and $\mathbf{2}^{6+}$ were readily purified by column chromatography (SiO_2: 2% w/v MeCN solution of NH_4PF_6 as the eluent), resulting in yields of 60 and 80%, respectively. It should be emphasised that, despite the fact that both $\mathbf{1}^{6+}$ and $\mathbf{2}^{6+}$ are composed of similar loops and tail components, we were interested as to whether the differences in the constitutions of their linkers, connecting the loops to their tails, would lead to differences in their conformational behaviour under reducing conditions. Specifically, in the case of $\mathbf{1}^{6+}$, the linker contains a relatively bulky imide group, whereas in the case of $\mathbf{2}^{6+}$, it is replaced by a much smaller ester function, increasing the freedom of motion of the substituted *p*-phenylene linker of the loop components, *e.g.*, the motion about its *para*-substituted axis. In the fully oxidised states, no interaction is present between the tail and the loop components in either $\mathbf{1}^{6+}$ or $\mathbf{2}^{6+}$, an observation which can be ascribed to the strong coulombic repulsion that surely exists between the $BIPY^{2+}$ units. By contrast, upon reduction, both $\mathbf{1}^{6+}$ and $\mathbf{2}^{6+}$ can accept three electrons readily to generate their corresponding trisradical tricationic states—namely $\mathbf{1}^{3(\bullet+)}$ and $\mathbf{2}^{3(\bullet+)}$—where it is possible, in principle at least, for them to undergo self-interlacing as a result of intramolecular radical-pairing interactions involving all three $BIPY^{\bullet+}$ units.

The self-complexing properties of $\mathbf{1}^{3(\bullet+)}$ and $\mathbf{2}^{3(\bullet+)}$ were first of all investigated by UV/Vis/NIR spectrophotometry. Following the reduction of $\mathbf{1}^{6+}$ to its radical state by Zn dust, the absorption spectra of a series of MeCN solutions, containing different concentrations of $\mathbf{1}^{3(\bullet+)}$ ranging from 10–80 μM, were recorded. It transpires (Fig. 2a) that at all concentrations, strong absorption bands centered upon 600 nm emerge, an observation which is a characteristic feature of the $BIPY^{\bullet+}$ radical cation. In addition, absorption bands centered on 900 nm grow in their intensities as well, suggesting that the radical-pairing interactions drive the formation of the $(BIPY^{\bullet+})_2$ radical dimer[33,34] rather than an intramolecular trisradical tricationic "complex". Moreover, the absorption intensities of these bands correlate (Fig. 2b) linearly with the concentration of $\mathbf{1}^{3(\bullet+)}$, an observation which indicates that pimerization[33] takes place intramolecularly in a side-on fashion, *i.e.*, the $BIPY^{\bullet+}$ unit of the tail folds back to interact in an alongside manner with one of the two $BIPY^{\bullet+}$ units in the loop component.

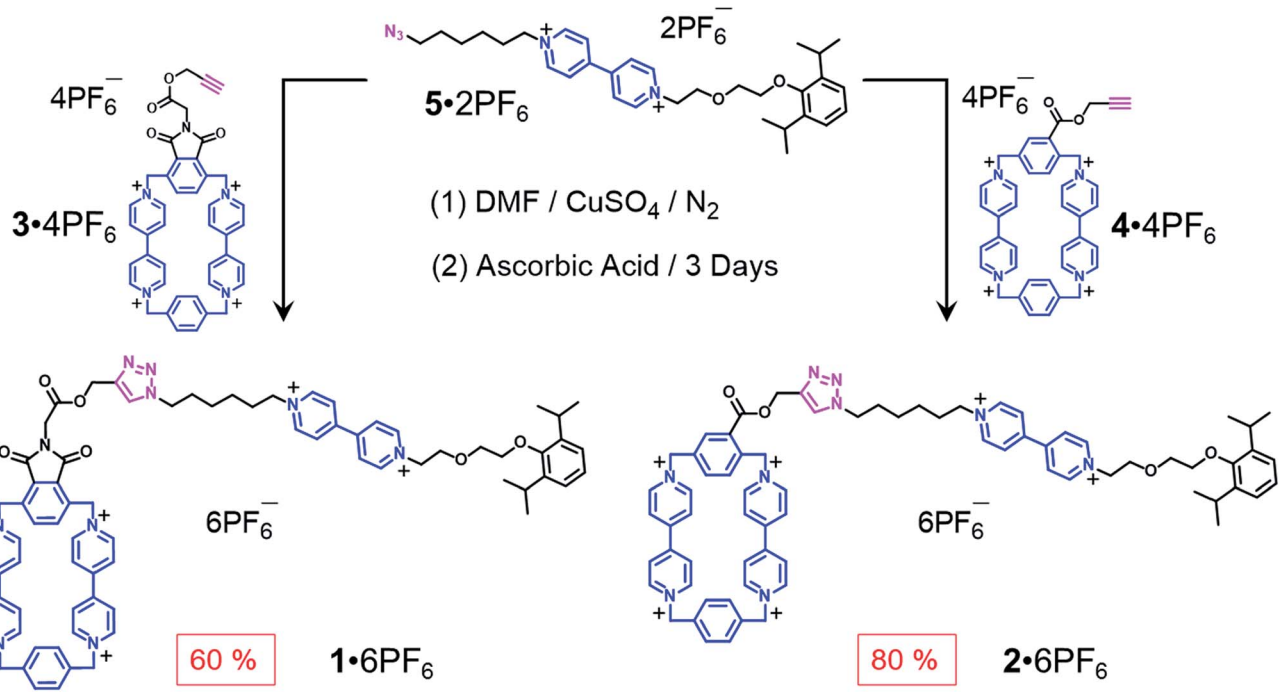

Scheme 1 Syntheses of the two potential viologen-based molecular lassos 1^{6+} and 2^{6+}.

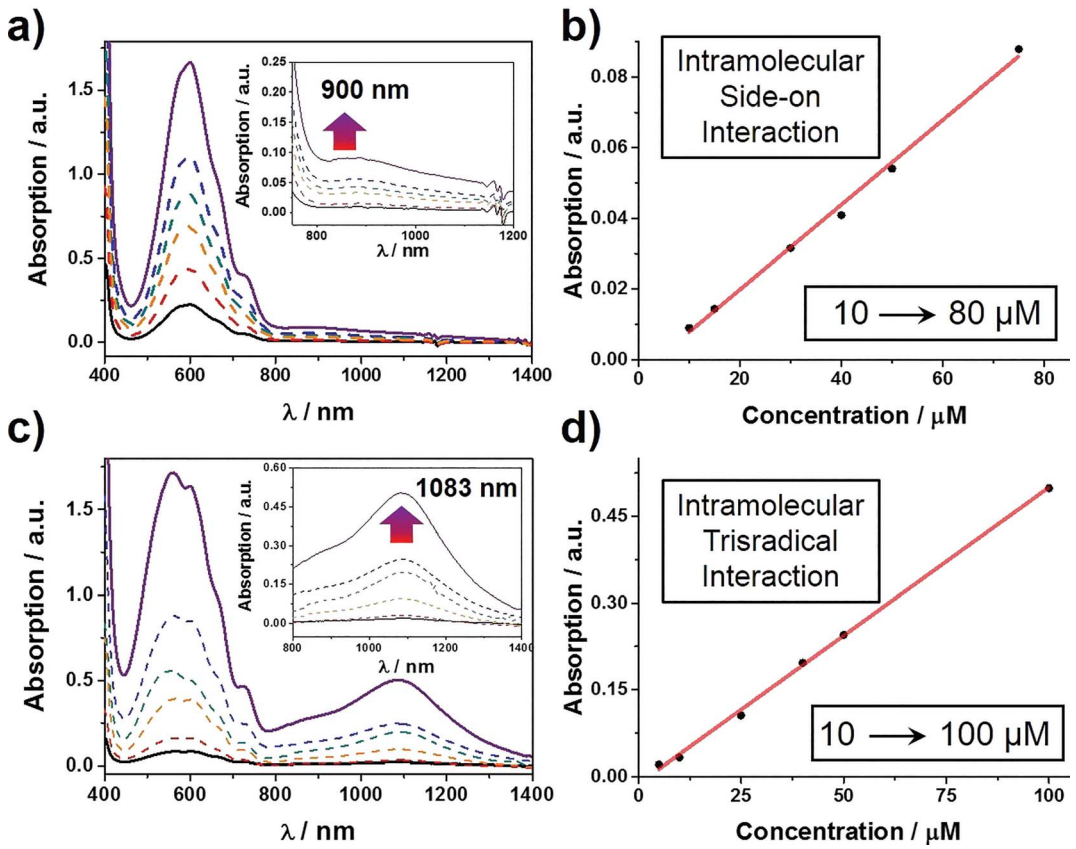

Fig. 2 UV/Vis/NIR absorption spectra of (a) $1^{3(\bullet+)}$ and (c) $2^{3(\bullet+)}$ recorded over a range of different concentrations. Dependence of the intensity of the band at (b) at 900 nm for $1^{3(\bullet+)}$ and (d) 1083 nm for $2^{3(\bullet+)}$ on concentration. In both cases, the linear relationships point to the fact that absorption bands result from intramolecular radical-pairing interactions.

By contrast, the MeCN solutions of $2^{3(\bullet+)}$ show (Fig. 2c) very different spectrophotometric behaviour. On treating the MeCN solutions of 2^{6+} with an excess of Zn dust, the solution turned dark purple within a minute. In comparison with the weak absorption bands observed around 900 nm in the case of $1^{3(\bullet+)}$, the spectra of $2^{3(\bullet+)}$ display strong absorption bands centered on 1083 nm, demonstrating unequivocally the formation of a tris-radical trication inclusion "complex". This process, which is more favoured than the side-on pimerization,[33] is also driven by intramolecular radical-pairing interactions. This conclusion is supported by the fact that the absorption intensities show (Fig. 2d) a linear dependency on concentration. Because of the existence of the bulky 2,6-diisopropylphenyl group at the terminus of the tail component, it follows that this interlaced pseudo[1]rotaxane-like conformation of $2^{3(\bullet+)}$ can only be accessed by an approach wherein the *p*-phenylene linker of the loop component experiences a revolving-door transformation, allowing the $BIPY^{\bullet+}$ unit in the tail to enter the cavity of the loop component, forming a molecular lasso. This mechanism also explains why the self-interlacing phenomenon is not observed in the case of $1^{3(\bullet+)}$, since it is hampered from occurring by the much bulkier imide function, *i.e.*, the door is prevented by its very size from revolving. Furthermore, in order to test the reversibility of these reduction-induced self-complexing processes, we exposed CD_3CN solutions containing $1^{3(\bullet+)}$ and $2^{3(\bullet+)}$, respectively, to oxygen in the air. ^1H NMR spectra were recorded during the time when their purple CD_3CN solutions turned colorless. The results show (see Section 9 in the ESI†) that, after the re-oxidation, the ^1H NMR spectra are almost identical to those recorded before reduction, indicating that the initial disentangled rope-like conformations of 1^{6+} and 2^{6+} are restored, thus confirming that these self-complexing processes can be driven reversibly by redox stimuli. It is also noteworthy that, when undergoing oxidation by the oxygen in the air, the CD_3CN solution of $2^{3(\bullet+)}$ demonstrates (see Section 10 in the ESI†) a higher resistance than that of $1^{3(\bullet+)}$ to the oxidation on account of its self-interlaced lasso-like conformation, a phenomenon which is reminiscent of the fact that lasso peptides exhibit[6] stability towards degradation by compounds in their vicinity.

In an attempt to elucidate the mechanism of electron transfer during the self-complexing processes of $1^{3(\bullet+)}$ and $2^{3(\bullet+)}$, cyclic voltammetry (CV) was performed. While the CV profile (Fig. 3, blue trace) of an equimolar mixture of 5^{2+} and 3^{4+} in MeCN indicates (see Section 4 in the ESI†) the formation of an inclusion complex, namely $5^{\bullet+} \subset 3^{2(\bullet+)}$, upon scanning the potential in a negative direction, this scenario is not observed (Fig. 3, red trace) in the case of 1^{6+}. The first broad peak at −434 mV, which is a combination of a two-electron, followed by a single-electron, reduction process corresponding to $1^{6+} \rightarrow 1^{3(\bullet+)}$, experiences significant cathodic shifts of 53 and 138 mV, respectively, compared with those (−381 and −296 mV) of the equimolar mixture of 5^{2+} and 3^{4+}, demonstrating that the radical species are less stable compared with the formation of the trisradical inclusion complex, an observation which is consistent with the hypothesis that two of the $BIPY^{\bullet+}$ units in $1^{3(\bullet+)}$ interact in a side-on fashion, giving rise to weaker

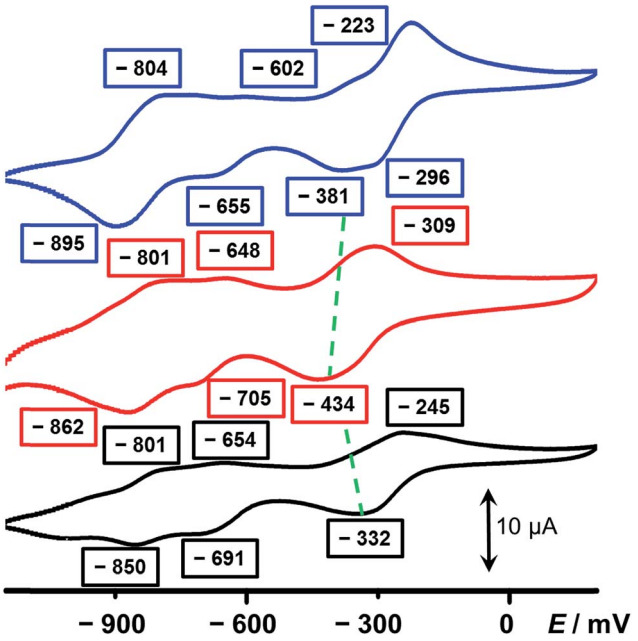

Fig. 3 Cyclic voltammograms of (i) an equimolar mixture of the half-dumbbell 5^{2+} and 3^{4+} (blue), (ii) 1^{6+} (red) and (iii) 2^{6+} (black). The green dashed lines denote the shifts in potentials between the complex and the two components. A glassy carbon working electrode, a platinum counter electrode, and a Ag/AgCl reference electrode were used in the characterisation of the MeCN solutions (0.1 mM for each component) at 298 K with 0.1 M $TBAPF_6$ serving as the electrolyte. A scan rate of 200 mV s^{-1} was used in all the analyses.

radical-pairing interactions. Since 3^{4+} has a higher reduction potential (Fig. S7†) than 5^{2+}, we believe that the ring component in 1^{6+} first of all receives two electrons, followed by the single-electron reduction of the half-dumbbell component, resulting in all the $BIPY^{2+}$ units being present in their radical cationic states. Next, the trisradical trication $1^{3(\bullet+)}$ accepts one electron at −705 mV and another two electrons at −862 mV to give the fully neutral state $1^{(0)}$.

The CV of 2^{6+} also reveals three sets of reduction peaks. Two of them, which emerge at −691 and −850 mV—corresponding to the $2^{3(\bullet+)}/2^{2(\bullet+)}$ and the $2^{2(\bullet+)}/2^{0}$ redox couples, respectively—have values close to those of 1^{6+}. The other reduction peak which emerges at −332 mV is also a combination of two successive reduction processes, involving $2^{6+} \rightarrow 2^{2(\bullet+)2+}$ and $2^{2(\bullet+)2+} \rightarrow 2^{3(\bullet+)}$, and showing a significant anodic shift compared with that of 1^{6+} and even the equimolar mixture. This observation can be ascribed to the fact that, once 2^{6+} is reduced to $2^{3(\bullet+)}$, the smaller-sized linker between the loop and the tail of the rope allow the trisradical "complexation" to take place immediately, consequently stabilising the radical species. On the other hand, since this process is an intramolecular one, the close proximity between the loop and the half-dumbbell component of the rope, compared with the equimolar mixture of 5^{2+} and 3^{4+}, facilitates the occupation by the $BIPY^{\bullet+}$ unit inside the cavity of the loop and gives rise to an even higher potential value than that of the mixture. The numbers of electrons involved in the reduction processes have been confirmed (see Section 8 in the ESI†) by differential pulse voltammetric

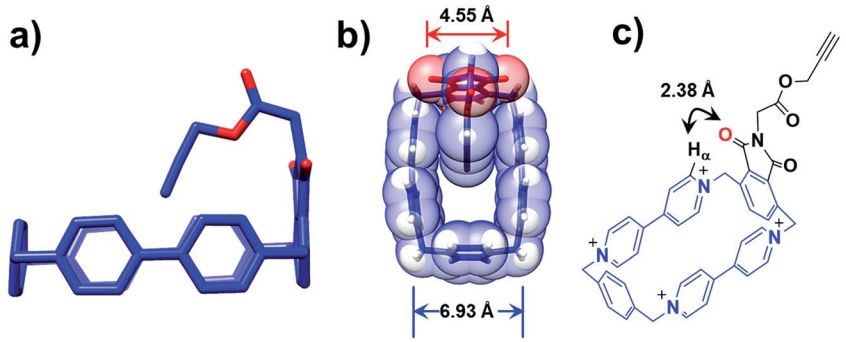

Fig. 4 Solid-state structure of the CBPQT^{4+} derivative 3^{4+} obtained by single-crystal X-ray crystallography. (a) Wireframe representation of 3^{4+} from a side-on perspective, which shows the alkyne group pointing inwards towards the centre of the loop. (b) Wireframe and space-filing representation from a plan perspective, where the distances between (i) the two oxygen atoms of the imide group and (ii) two centroids of the BIPY^{2+} units are shown. (c) A short distance contact between the H_α on the BIPY^{2+} unit and O atom of the imide is shown. The PF_6^- counterions are omitted for the sake of clarity.

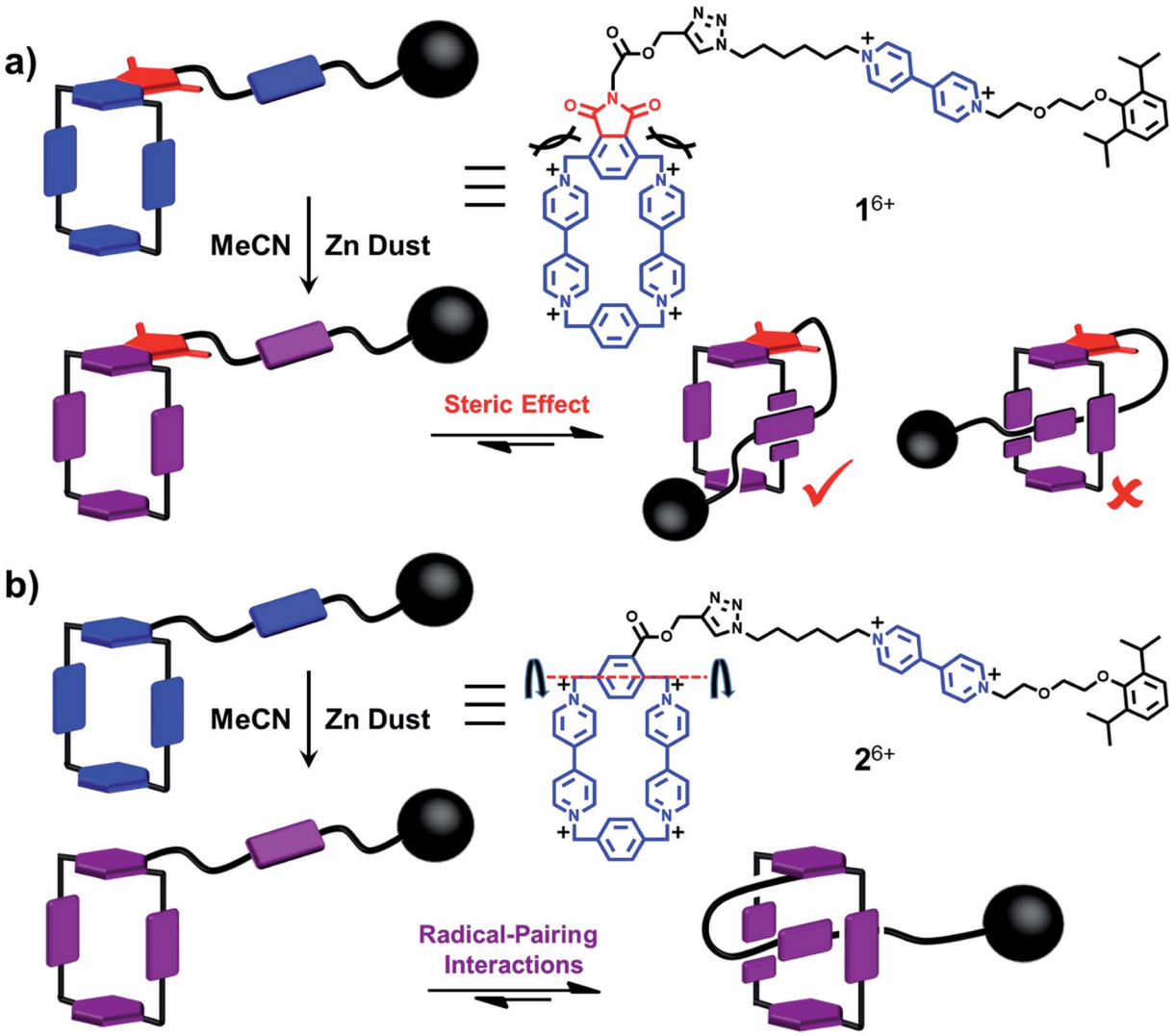

Fig. 5 A schematic summary of the reduction-induced motions in the potential viologen-based molecular lassos 1^{6+} and 2^{6+}. (a) Conversion of 1^{6+} to its reduced state, $1^{3(\bullet+)}$, by treating with Zn dust, where the self-entanglement is prohibited because of the disfavoured steric repulsion and only a side-on interacting mode is allowed. (b) Conversion of 2^{6+} to its reduced state, $2^{3(\bullet+)}$, by treating with Zn dust, which triggered a self-entanglement process to form a lasso-like pseudo[1]rotaxane with a noose-like conformation, as a result of strong intramolecular radical-pairing interactions.

(DPV) experiments. In all, the conclusions drawn from the CV are in a good agreement with the observations made from the UV/Vis/NIR spectra, illustrating the fact that subtle structural differences between $\mathbf{1}^{6+}$ and $\mathbf{2}^{6+}$ lead to their having very different molecular-level properties in their radical states. While $\mathbf{2}^{6+}$ can form a self-interlaced lasso-like conformation by means of a revolving-door mechanism, a similar change in conformation is precluded by the bulkier linker in its analogue $\mathbf{1}^{6+}$, leaving an unthreaded conformation with a side-on interaction between the loop and the tail of the rope as the only alternative.

Further insight into how the structural differences affect the binding modes of $\mathbf{1}^{6+}$ under reducing conditions comes from single-crystal X-ray crystallography. Single crystals of $\mathbf{3}^{4+}$, suitable for X-ray crystallographic analysis, were obtained from slow vapor diffusion of $i\mathrm{Pr}_2\mathrm{O}$ into an MeCN solution (1 mM) of $\mathbf{3}^{4+}$ during one week at room temperature. The solid-state structure reveals that the loop retains its rectangular shape in the presence of the imide functional group, while the alkyne-terminated tail is orientated (Fig. 4a) inwards toward the centre of the loop. The centroid-to-centroid distance between the two BIPY^{2+} units is (Fig. 4b) 6.93 Å, while the span between the two oxygen atoms of the imide group is 4.55 Å. It has been shown[25,35,36] that the dimensions of the CBPQT^{4+} loop are barely affected at all by its redox states, making it reasonable to assume that these distance parameters in $\mathbf{3}^{4+}$ remain unchanged when it is reduced to $\mathbf{3}^{2(\bullet+)}$. As a consequence, in the case of $\mathbf{1}^{3(\bullet+)}$, when the imide-attached *p*-phenylene function attempts to undergo the revolving-door route to form the lasso-like pseudo[1]rotaxane, a high-energy conformation where only *ca.* 1.20 Å separates the oxygen atom and the plane of the BIPY^{2+} units in the CBPQT^{4+} loop is generated, disfavouring self-entanglement. In addition, a close contact (2.38 Å) between the oxygen atom on the imide and the H_α proton of the BIPY^{2+} unit is observed (Fig. 4c), further disfavouring the revolving-door mechanism since (i) the hydrogen bonding interactions between the oxygen atom and the H_α proton in this conformation have to be broken, and (ii) it is apparent that the imide group will be hindered sterically first of all by the H_α proton before reaching into the centre of the loop as a result of the revolving-door mechanism. Taken together, these geometric parameters observed in the solid-state structures of $\mathbf{3}^{4+}$ confirm that the lasso-like pseudo[1]rotaxane conformation in the case of $\mathbf{1}^{3(\bullet+)}$ is not accessible.

Conclusions

In summary, two potential molecular lassos, $\mathbf{1}^{6+}$ and $\mathbf{2}^{6+}$, which respond to both chemical and electrochemical stimuli as a consequence of the recognition between the $\mathrm{BIPY}^{\bullet+}$ radical cations, have been prepared. Their self-complexing properties under reducing conditions, designed to mimic those of the lasso peptides, have been investigated in considerable detail. UV/Vis/NIR spectrophotometric and electrochemical studies, along with single crystal X-ray crystallography, reveal that, in the case of $\mathbf{1}^{3(\bullet+)}$, the bulky imide group linking the loop and the half-dumbbell component of the rope only allows (Fig. 5a) the $\mathrm{BIPY}^{\bullet+}$ groups in the loop and the tail of the rope to "dimerise" in a side-on interacting fashion. In comparison, the smaller-size linker in $\mathbf{2}^{3(\bullet+)}$ renders it possible to form (Fig. 5b) a mechanically interlocked lasso-like pseudo[1]rotaxane conformation, employing a revolving-door mechanism on the part of the *p*-phenylene ring. More importantly, this self-interlacing behaviour, driven by intramolecular trisradical tricationic interactions, is reversible upon changing the external potentials, as evidenced by both cyclic voltammetry and ^{1}H NMR spectroscopy. In conclusion, we have made two potential molecular lassos, one of which can switch reversibly between disentangled and self-entangled states, and in so doing form a noose, reminiscent of lasso peptides. Besides, by comparing the different actuating mechanisms of these two potential viologen-based molecular lassos, we demonstrate how the molecular-level properties of analogous compounds can be affected drastically by subtle structural differences, while shedding light on the synthesis of a molecular lasso with a well-designed and finely tuned means of actuating it.

Acknowledgements

This research is part of the Joint Center of Excellence in Integrated Nano-Systems (JCIN) at King Abdulaziz City for Science and Technology (KACST) and Northwestern University (NU). The authors would like to thank both KACST and NU for their continued support of this research.

References

1 M. O. Maksimov, S. J. Pan and A. J. Link, *Nat. Prod. Rep.*, 2012, **29**, 996.
2 J. D. Hegemann, M. Zimmermann, X. Xie and M. A. Marahiel, *Acc. Chem. Res.*, 2015, **48**, 1909.
3 C. Clavel, K. Fournel-Marotte and F. Coutrot, *Molecules*, 2013, **18**, 11553.
4 J. E. Velásquez and W. van der Donk, *Curr. Opin. Chem. Biol.*, 2011, **15**, 11.
5 K. Kuznedelov, E. Semenova, T. A. Knappe, D. Mukhamedyarov, A. Srivastava, S. Chatterjee, R. H. Ebright, M. A. Marahiel and K. Severinov, *J. Mol. Biol.*, 2011, **412**, 842.
6 I. Mathavan, S. Zirah, S. Mehmood, H. G. Choudhury, C. Goulard, Y. Li, C. V. Robinson, S. Rebuffat and K. Beis, *Nat. Chem. Biol.*, 2014, **10**, 340.
7 M. O. Maksimov and A. J. Link, *J. Am. Chem. Soc.*, 2013, **135**, 12038.
8 C. Reuter, A. Mohry, A. Sobanski and F. Vögtle, *Chem.–Eur. J.*, 2000, **6**, 1674.
9 K. Hiratani, M. Kaneyama, Y. Nagawa, E. Koyama and M. Kanesato, *J. Am. Chem. Soc.*, 2004, **126**, 13568.
10 Y. Liu, A. H. Flood, R. M. Moskowitz and J. F. Stoddart, *Chem.–Eur. J.*, 2005, **11**, 369.
11 X. Ma, D. Qu, F. Ji, Q. Wang, L. Zhu, Y. Xu and H. Tian, *Chem. Commun.*, 2007, 1409.
12 N. L. Strutt, H. Zhang, M. A. Giesener, J. Lei and J. F. Stoddart, *Chem. Commun.*, 2012, **48**, 1647.
13 C. Clavel, C. Romuald, E. Brabet and F. Coutrot, *Chem.–Eur. J.*, 2013, **19**, 2982.

14 G. W. Gokel, *Chem. Soc. Rev.*, 1992, **21**, 39.
15 G. W. Gokel, W. M. Leevy and M. E. Weber, *Chem. Rev.*, 2004, **104**, 2723.
16 Q. Zhou, P. Wei, Y. Zhang, Y. Yu and X. Yan, *Org. Lett.*, 2013, **15**, 5350.
17 H. Li, X. Li, H. Agren and D.-H. Qu, *Org. Lett.*, 2014, **16**, 4940.
18 P. W. C. Clavel, K. Fournel-Marotte and F. Coutrot, *Chem. Sci.*, 2015, **6**, 4828.
19 A. Miyawaki, P. Kuad, Y. Takashima, H. Yamaguchi and A. Harada, *J. Am. Chem. Soc.*, 2008, **130**, 17062.
20 L. Zhu, H. Yan and Y. Zhao, *Int. J. Mol. Sci.*, 2012, **13**, 10132.
21 S. Di Motta, T. Avellini, S. Silvi, M. Venturi, X. Ma, H. Tian, A. Credi and F. Negri, *Chem.–Eur. J.*, 2013, **19**, 3131.
22 Z. Xue and M. F. Mayer, *J. Am. Chem. Soc.*, 2010, **132**, 3274.
23 Y. Liu, S. Saha, S. A. Vignon, A. H. Flood and J. F. Stoddart, *Synthesis*, 2005, **18**, 3437.
24 A. Trabolsi, N. Khashab, A. C. Fahrenbach, D. C. Friedman, M. T. Colvin, K. K. Cotí, D. Benítez, E. Tkatchouk, J.-C. Olsen, M. E. Belowich, R. Carmielli, H. A. Khatib, W. A. Goddard III, M. R. Wasielewski and J. F. Stoddart, *Nat. Chem.*, 2010, **2**, 42.
25 A. C. Fahrenbach, J. C. Barnes, D. A. Lanfranchi, H. Li, A. Coskun, J. J. Gassensmith, Z. Liu, D. Benítez, A. Trabolsi, W. A. Goddard III, M. Elhabiri and J. F. Stoddart, *J. Am. Chem. Soc.*, 2012, **134**, 3061.
26 C. J. Bruns, M. Frasconi, J. Iehl, K. J. Hartlieb, S. T. Schneebeli, C. Cheng, S. I. Stupp and J. F. Stoddart, *J. Am. Chem. Soc.*, 2014, **136**, 4714.
27 Y. Wang, M. Frasconi, W.-G. Liu, J. Sun, Y. Wu, M. S. Nassar, Y. Y. Botros, W. A. Goddard III, M. R. Wasielewski and J. F. Stoddart, *ACS Cent. Sci.*, 2016, **2**, 89.
28 J. M. Rawson, A. Alberola and A. Whalley, *J. Mater. Chem.*, 2006, **16**, 2560.
29 Y. Liu, C. Chipot, X. Shao and W. Cai, *J. Phys. Chem. C*, 2014, **118**, 19380.
30 C. Romuald, A. Ardá, C. Clavel, J. Jiménez-Barbero and F. Coutrot, *Chem. Sci.*, 2012, **3**, 1851.
31 C. Romuald, G. Cazals, C. Enjalbal and F. Coutrot, *Org. Lett.*, 2013, **15**, 184.
32 J.-C. Chang, S.-H. Tseng, C.-C. Lai, Y.-H. Liu, S.-M. Peng and S.-H. Chiu, *Nat. Chem.*, 2017, **9**, 128.
33 W. Geuder, S. Hünig and A. Suchy, *Tetrahedron*, 1986, **42**, 1665.
34 T. M. Bockman and J. Kochi, *J. Org. Chem.*, 1990, **55**, 4127.
35 B. Odell, M. V. Reddington, A. M. Z. Slawin, N. Spencer, J. F. Stoddart and D. J. Williams, *Angew. Chem., Int. Ed. Engl.*, 1988, **27**, 1547.
36 M. Frasconi, I. R. Fernando, Y. Wu, Z. Liu, W.-G. Liu, S. M. Dyar, G. Barin, M. R. Wasielewski, W. A. Goddard III and J. F. Stoddart, *J. Am. Chem. Soc.*, 2015, **137**, 11057.